Coupling starlight into single-mode photonic crystal fiber using a field lens

Jason C.W. Corbett and Jeremy R. Allington-Smith

Centre for Advanced Instrumentation, Durham University, Dept of Physics South Road Durham
j.c.w.corbett@durham.ac.uk, j.r.allington-smith@durham.ac.uk

Abstract: We determine the coupling characteristics of a large mode area (LMA) photonic crystal, single-mode fiber when fed with an on-axis field lens used to place an image of the telescope exit pupil at the fiber input. The maximum field of view is found to be approximately the same as that of feeding the fiber directly with the telescope PSF in the image plane. However, the field lens feed can be used to provide a flat, maximised coupling response over the entire visible-NIR which is not possible using either the highly wavelength dependent direct feed coupling to the LMA fiber or the attenuation spectrum limited step index fiber cases.

OCIS Codes: (350.1260) Astronomical optics; (120.3180) Interferometry; (060.2430) Fibers, single-mode; (999.999) Photonic crystal fiber; (100.2960) Image analysis.

References

1. T. Birks, J. Knight and P St. J Russell, "Endlessly single-mode photonic crystal fiber," Opt. Lett., **22** p 961-963 (1997)
2. E.G. Neumann, *Single-Mode Fibers – Fundamentals*, (Springer-Verlag, 1988)
3. A. Bjarklev, J. Broeng, A.S. Bjarklev, *Photonic crystal fibers, (*Kluwer, 2003)
4. Coude de Foresto, V. Ridgway S., Mariotti J.M, "Deriving object visibilities from interferograms obtained with a fiber stellar interferometer,"A&AS **121** 379 (1997)
5. G. Perrin, O. Lai, P. J. Lena, and V. Coude du Foresto, "Fibered large interferometer on top of Mauna Kea: OHANA, the Optical Hawaiian Array for Nanoradian Astronomy," in *Interferometry in Optical Astronomy*, P. J. Lena and A. Quirrenbach, eds.,Proc. SPIE **4006,** 708–714 (2000).
6. M.D. Nielson, J.R. Folkenberg, N.A. Mortenson and A. Bjarklev, "Bandwidth comparison of photonic crystal fibers and conventional single-mode fibers," Opt. Express **12**, 430 (2004) http://www.opticsexpress.org/abstract.cfm?URI=OPEX-12-3-430
7. M.D. Nielsen, N.A. Mortensen, M. Albersen, J.R. Folkenberg, A. Bjarklev, D. Bonacinni, "Predicting macrobending loss for large-mode area photonic crystal fibers," Opt. Express **12**, 1775 (2004) http://www.opticsexpress.org/abstract.cfm?URI=OPEX-12-8-1775
8. A.W. Snyder and J.D. Love, *Optical waveguide Theory*, (Chapman/Kluwer, 1983/ 2000)
9. Joseph W Goodman, *Introduction to Fourier Optics, (* McGraw-Hill, 1996)
10. T.P. White, B.T. Kuhlmey, R.C. McPhedran, D. Maystre, G. Renversez, C. Martijn de Sterke, L.C. Botton, "Multipole method for microstructured optical fiber. I Formulation," J. Opt. Soc. Am. B **19** , No 10 (2002)
11. B.T. Kuhlmey, T.P. White, G. Renversez, D. Maystre, L.C. Botton, C. Martijn de Sterke, R.C. McPhedran, "Multipole method for microstructured optical fiber. II Implementation and Results," J. Opt. Soc. Am. B **19** , No 10 (2002)
12. M.J Steel, T.P White, C. Martijn de Sterke, R.C. McPhedran, L.C. Botton, "Symmetry and degeneracy in microstructered optical fibers," Opt. Lett. **26** No.8 (2001).
13. D.T. Liu, B.M. Levine & M. Shao, "Design and fabrication of a coherent array of single-mode optical fibers for the nulling coronograph,"Proc. SPIE **5170** Techniques and Instrumentation for detection of exoplanets. (2003)
14. N.A. Mortensen and J.R. Folkenberg, "Near-field to far-field transition of photonic crystal fibers: symmetries and interference phenomena," Opt. Express **10**, 475 (2002).http://www.opticsexpress.org/abstract.cfm?URI=OPEX-10-11-475
15. Born and Wolf, *Principles of optics* 7th edition, (Cambridge University Press)**.**
16. A. Snyder, "Excititation and scattering of modes on a dielectric optical fiber," IEEE Trans. MTT V NIT-**17** No.12 (1969)
17. Equation (8) actually underestimates slightly $\rho < 0.40$ for >f/4 and $\lambda_o > 1000$nm when coupling into the LMA-8 fiber however no simple model can account for the actual variation and direct recourse to Eq. (1) and (6) is required.
18. Olivier Guyon, "Wide-field interferometric imaging with single-mode fibers," A&A **387**, 366-378 (2002)

#7947 - $15.00 USD Received 27 June 2005; revised 11 August 2005; accepted 11 August 2005

1. Introduction

1.1 Large mode area (LMA) photonic crystal fiber.

LMA fibers are a type of photonic crystal fiber whereby optical energy is trapped and guided by a crystal structure [1], see Fig.1, rather than the step reduction in refractive index between core and cladding of a traditional step index fiber [2]. See Refs. [1] and [3] for full details but in basic terms the LMA fiber crystal structure can be thought of as having a lower bulk refractive index than the core. Light is thus trapped in the central defect (missing hole) and guided along the fiber.

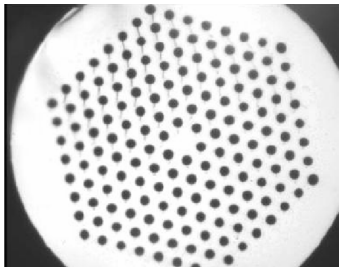

Fig. 1. Cross section of an LMA type fiber – Crystal Fiber A/S

Whilst the crystal structure acts as a boundary and can be thought of as having the same function as the step in refractive index for traditional fibers, it does behave differently to a simple step and it is this behavior that gives LMA type fibers their unique properties. Primarily the average effective index of the photonic structure is far more wavelength dependent than a simple step. As the wavelength of the guided light decreases the effective index of the crystal structure approaches the index of the silica from which it is made and hence the difference between core and cladding index reduces. Thus as the width of the fundamental mode tries to decrease at higher energies, the refractive index change in the photonic structure causes the mode to spread back out. Therefore not only is the mode size (to a good approximation) independent of wavelength, but the fiber is also *endlessly single-moded* over all wavelengths at which silica (from which most commercially available fiber are made) is transparent.

This is in contrast to the step index case which is only singlemoded for wavelengths above its cutoff (below which the fiber becomes multimoded) and generally have a very limited bandwidth whereas, LMA fibers generally have a very low attenuation spectrum (i.e., loss as a function of wavelength and fiber length) over a very broad waveband. For instance the LMA-8 through to LMA-20 made by Crystal Fiber A/S can be used to simultaneously couple visible and NIR at less than 10db/km attenuation, excepting the peak at 1400nm due to OH.

Further to this, the characteristic scale of the photonic crystal is much larger than step index fibers and hence much larger core sizes are a feature. The LMA-20 fiber, for instance, has a mode size of ~15-16μm compared to a typical step index fiber fundamental mode size of 2-3μm at 400nm .

1.2 Single-mode fibers in interferometry

Step index single-mode fibers are used in stellar interferometry to coherently couple light from multiple apertures and to provide spatial filtering of atmospherically aberrated wavefronts – see [4] and the references therein. However, the attenuation spectrum of step index fibers is generally limited to the 1.05 to 1.35 λ/λ_{cutoff} region where λ_{cutoff} is the singlemode cutoff wavelength, below which the fiber becomes multimoded. In the VIS this equates to a useable spectral range of about 200nm or so and hence a range of fibers and feed optics is required for broad band interferometry [5]. The broad attenuation spectrum [6] and endlessly singlemoded behavior of LMA fibers thus provides a significant advantage over step index fibers allowing coupling of the entire VIS-NIR into a single fiber.

#7947 - $15.00 USD Received 27 June 2005; revised 11 August 2005; accepted 11 August 2005

Both step index and LMA fibers suffer from an upper bendloss edge in their attenuation spectra associated with the radiation of the tail of the transverse modal field on the outside of a bend of some radius as at some distance from the fiber axis its local velocity vector exceeds the local speed of light [2]. However, the reducing difference between the bulk refractive index of the cladding with respect to the core of the LMA fiber [3], which accounts for most this fibers interesting properties, also leads to a lower bendloss edge. The position of the edge is a function of the scale (and geometry) of the fiber [7] and care needs to be taken to match the correct fiber to the application to avoid either excessive bendlosses or unnecessarily stringent minimum bend radii in the fiber run.

The mode field of LMA fibers is typically at least twice the size of traditional step index fibers. For example, the Nufern 460HP is optimised for use in the range 450nm-600nm with an MFD of 4 μm, whereas the Crystal Fiber A/S LMA-8, optimised for vanishing bendloss at >350nm for a 4cm minimum bend radius, has an MFD of 8μm, which should be somewhat easier to align to optically. Note also that if the LMA fiber can be restricted to a minimum bend radii of >16cm or so then an LMA-15 fiber could be used to usefully transmit at >450nm. The LMA-16 has an MFD of 15μm, nearly four times that of the step index alternative.

Since the mode field diameter of LMA fibers is approximately independent of wavelength we investigate the coupling of starlight into LMA type fibers of arbitrary characteristic scale, Λ, using an on axis field lens, placed in the image plane of the telescope and illuminating the fiber endface with a conjugate telescope exit pupil image. The results of this analysis are compared to the direct feed case, i.e., feeding the fiber directly from the image plane in Section 4.

2. Coupling model

The lenslet coupling case is shown in Fig. 2. The field lens in *i'* places an image of the telescope exit pupil on the endface of the fiber. The field assignments for the lenslet feed in Fig. 2(b) assume that the telescope and its foreoptics, which provides magnification, *M*, are subsumed into one element such that $\mathbf{E}_d$ is the electric field incident on the telescope entrance pupil, and since we consider only unabberrated optical components, $\mathbf{E}'_d$ is the resulting spherical field converging toward the image plane, *i'* and it is this field that acts as the coherent object for the field lenslet. *n* is the refractive index of the space immediately in front of the fiber. **E** is the spherical wavefront diverging from some arbitrary point (ε,η) in $\mathbf{E}'_d$ and **E'** is the spherical wavefront converging from the lenslet to the point (p,q) in the image field $\mathbf{E}_i$ at the fiber endface. Throughout this work, bold type indicates a complex field and is retained for fields that can be taken as completely real for brevity.

In the direct feed case, the lenslet is removed and the endface of the fiber placed in the image plane, *i'*.

#7947 - $15.00 USD Received 27 June 2005; revised 11 August 2005; accepted 11 August 2005

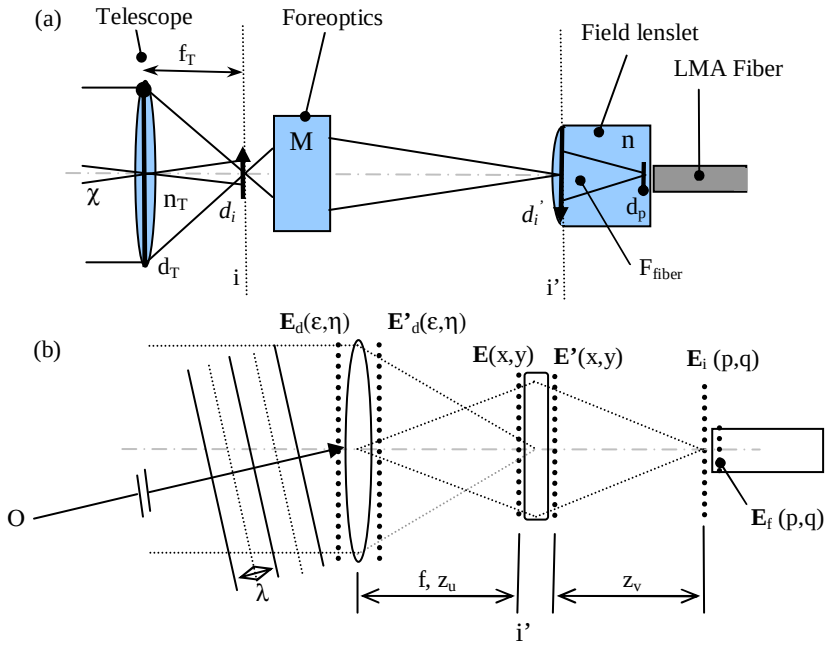

Fig. 2. The Telescope-Fiber feed (a) Schematic (b) Field assignment

The coupling efficiency between the incident field $\mathbf{E}_i$ (whether the Airy pattern of the direct feed or the electric field of the pupil image) and fiber mode field $\mathbf{E}_f$ is given by the coupling integral (1),

$$\rho = \frac{\left| \int_A \mathbf{E}_i \mathbf{E}_f^* \, dA \right|^2}{\int_A \left| \mathbf{E}_i \right|^2 dA \int_A \left| \mathbf{E}_f \right|^2 dA} \tag{1}$$

where, A is the area defined by the infinite *(x-y)* plane transverse to the optical axis (z). Full derivations of this equation are given for smoothly varying or step index fibers in references [2] and [8]. While a complete analysis of the validity of this formula for LMA type fibers is beyond the scope of this paper, this approach can be applied to commercially available LMA fibers which have many rings of holes in their cross sectional structure surrounding the central defect and thus have well bound guided modes. In this case, A, may be taken as the real plane transverse to the fiber axis and located at z=0, the fiber endface. All modes (guided and radiated) can be shown to be orthogonal over A and this condition together with the requirement that the tangential components of the **E** and **H** fields are continuous across the fiber endface boundary can be used to isolate the power coupled into the transverse modal fields of the fiber. This paper deals only with the case where the back reflected field $\mathbf{E}_r$ and therefore its effect on the distribution of the input field $\mathbf{E}_i$ is negligible. In the case where $n \neq n_{core}$, where n is the refractive index in the plane of $\mathbf{E}_i$, and n_{core} that of the material from which the fiber is made, the overall coupling must be multiplied by the Fresnel transmission coefficient, $T = 4n.n_{core}/(n+n_{core})^2$.

The direct feed Airy pattern field magnitude is given by

#7947 - $15.00 USD Received 27 June 2005; revised 11 August 2005; accepted 11 August 2005

$$\mathbf{E}_i(\mathbf{r}) = \frac{J_1\left(k|\mathbf{r}|/2F\right)}{\left(k|\mathbf{r}|/2F\right)} - \varepsilon^2 \frac{J_1\left(\varepsilon k|\mathbf{r}|/2F\right)}{\left(\varepsilon k|\mathbf{r}|/2F\right)} \tag{2}$$

where $\mathbf{r} = (p,q)$ and F is the feed focal ratio into (p,q) the plane, k is the local wavenumber at the fiber endface and ε is the obscuration due to the telescope secondary such that $\varepsilon \in [0,1]$.

In the field lenslet case, the relationship between, $\mathbf{E}_i$ and $\mathbf{E}_d$ can be derived using the coherent imaging Eq. (3) as derived by Goodman[9],

$$\mathbf{E}_i(p,q) = \int_{-\infty}^{\infty}\int \mathbf{h}(p,q;\varepsilon,\eta)\mathbf{E}'_d(\varepsilon,\eta)d\varepsilon d\eta \tag{3}$$

where $\mathbf{h}$ is the system transfer function,

$$\mathbf{h}(p,q;\varepsilon,\eta) = \exp\left(i\frac{k_o}{2z_v}\left(p^2+q^2\right)\right)\exp\left(i\frac{k_o}{2z_U}\left(\varepsilon^2+\eta^2\right)\right)$$

$$\times \int_{-\infty}^{\infty}\int A(x,y)\exp\left(i\frac{k_o}{2z_v}\left((p-M\varepsilon)+(q-M_p\eta)\right)\right)dxdy \tag{4}$$

where, M is the magnification of the foreoptics and lenslet with respect to the telescope exit pupil and its (geometric) image on the fiber endface and $A(x,y)$ is the aperture stop of the lenslet. Z_u and Z_v are defined in Fig. 2 and the constant amplitude and phase terms have been ignored since they cancel in (1) and k_o is the free space wavelength.

$\mathbf{E}'_d$ converges toward the entrance pupil of the lenslet and $\mathbf{E}_d$ and $\mathbf{E}'_d$ are related by the paraxial approximation

$$\mathbf{E}'_d = \mathbf{E}_d \exp\left(-i\frac{\pi}{\lambda f}\left(\varepsilon^2+\eta^2\right)\right) \tag{5}$$

where f is distance between the exit pupil of the telescope/foreoptics combination and the plane i'and the exponential in Eq. (5) cancels exactly with the quadratic phase term in (ε,η) in Eq. (4).

The quadratic phase term in (p,q) describes the projection of the spherical image space, centered on the exit pupil of the lenslet, onto the (p,q) plane.

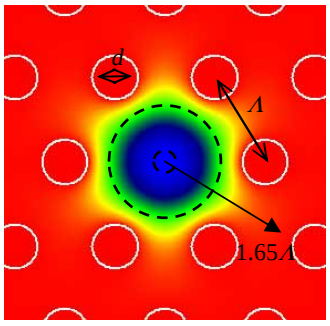

Fig. 3. Transverse field magnitude $|\mathbf{E}_f|$, represented on a linear scale, showing Λ the characteristic length of the photonic structure and overplotted outline of $\mathbf{E}_g(p,q)$, the geometric image of the exit pupil of the telescope shown at the correct scale of outer diameter ~ 1.33Λ for maximum coupling (Section 3.1)

From Fig. 3, points $|\mathbf{r}|^2 = |p^2+q^2| > 1.65\Lambda$ have magnitude less than 10^{-4} the peak value at the centre of the mode and thus changes in $\mathbf{E}_i$ at this point have a minimal effect on the

#7947 - $15.00 USD Received 27 June 2005; revised 11 August 2005; accepted 11 August 2005

numerator in (1). By computing its value over the endface of the fiber, the change in the (p,q) quadratic phase term can be shown to be negligible at $|\mathbf{r}| \leq 1.65\Lambda$ if the focal length of the lenslet, $f > 16\Lambda$, when the lenslet is in contact with the fiber (n=1.45) and $f > 13\Lambda$ for n = 1.00. The fastest lens(lets) considered in this work have focal ratios of f/2 implying a minimum aperture size of ~185μm for the LMA-35, ~105μm for the LMA-20 and ~45μm for the LMA-8 for the n=1.45 case, so the restriction is of little practical interest unless the very smallest of lenslets is used.

Note that this is more than just a range of validity on this model. The *(p,q)* quadratic phase term in the electric field will affect the maximum coupling efficiency by introducing a phase mismatch between $\mathbf{E}_i$ and the transverse component of $\mathbf{E}_f$.

With the quadratic phase terms removed, (3) and (4) can be shown [9] to reduce to the convolution of the amplitude point spread function $\mathbf{h}(p,q)$ of the exit aperture, $P(x,y)$ with the geometric image $\mathbf{E}_g(p,q)$ (Fig.2(b)), of $\mathbf{E}_d(\varepsilon,\eta)$ in the (p,q) plane,

$$\mathbf{E}_i(p,q) = \mathbf{h}(p,q) \otimes \mathbf{E}_g(p,q) \tag{6}$$

This formula forms the basis for the numerical results in the following sections. The **E** fields were computed on a 1000^2 array and after numerical trials a simple midpoint integration routine was found to yield the most stable and accurate results matching analytical examples to within +/-1%. An analytical approximation to the mode field of the fiber exists[14], however, we found that it introduces an added systematic error of +/-3%, in this application, by comparison to the numerically computed modes of the multipole method[10,11] and so the numerical method is used throughout. Also, we consider only circular field lenses.

A weak relationship exists [1,3] between mode field and wavelength, with both the mode 'size' and field distribution varying very slightly with wavelength. This results in a variation in coupling due to changes in the mode field (i.e., overall size and distribution). However this effect is characterised by changes in coupling of $<10^{-6}$ per nm and is therefore considered negligible.

The mode field of the LMA type fiber is actually a polarisation doublet[12]. That is, the total mode is actually composed of two orthogonally polarised modes of the same propagation constant. For azimuthally symmetric step index fibers, the mode field distribution of these two modes is identical and hence coupling into the fiber is completely independent of the polarisation of the incident field. However, the two fields of the LMA fiber show very slight differences due to the six-fold symmetry of the photonic structure and the need to match the boundary conditions of the field at the silica/air-hole boundaries. However, we have found that the difference in coupling efficiency in coupling in various pupil scales and obscurations to be of the order of 10^{-4} worst case with typical differences of 10^{-5}. Hence we take the LMA fiber to be completely polarisation independent in this respect.

Finally, the mode field of the fiber is non-azimuthally symmetric as shown in Fig. 4(a), however we find that the coupling efficiency changes by fractions of a percent with polarisation of $\mathbf{E}_i$ with respect to the polarisation doublet $\mathbf{E}_f$ and thus the polarisation of $\mathbf{E}_i$ is ignored throughout. Further, the effect of rotation of spiders of width ≤ 5% of the diameter of the telescope primary mirror has also been found to be negligible.

3. Characteristics of the field lens feed

This section quantifies the coupling efficiency due to parameters such as pupil image scale, telescope obscuration, incident wavelength which are seen to affect primarily the maximum coupling value (Section 3.1) and changes in coupling due to increasing input angle at the telescope are then found and used to derive the field of view (FOV) of this configuration. (Section 3.2).

3.1 On axis source

Figure 4 shows a 3D representation of the field magnitude of the fiber mode and an overplot of cross sections of the fiber mode and incident field, through their shared axis. The geometric

#7947 - $15.00 USD Received 27 June 2005; revised 11 August 2005; accepted 11 August 2005

image of the pupil, $\mathbf{E}_g$ of diameter d_p, Fig. 2(a), on the endface of the fiber is shown as the undiffracted case. As the focal ratio of the lenslet increases or the wavelength increases for the same lenslet, the subsequent size of the lenslet PSF, $\mathbf{h}(p,q)$ with respect to $\mathbf{E}_g$ increases and as the cross sections in the figure show, d_p is generally small enough, for any commercially available fiber, that the convolved pupil image, $\mathbf{E}_i(p,q)$, Eq. (6) can be significantly affected.

The least and most diffracted cases in the figure are of an *f*/2 lenslet at λ=400nm and an *f*/4 lenslet at λ=2000nm, respectively. The aperture of the lenslet will partially vignette the PSF of the telescope causing a loss in total throughput. However this does not effect the coupling efficiency *at the fiber* and hence is explained fully and quantified in Sections 3.2 and 4 and ignored for clarity here.

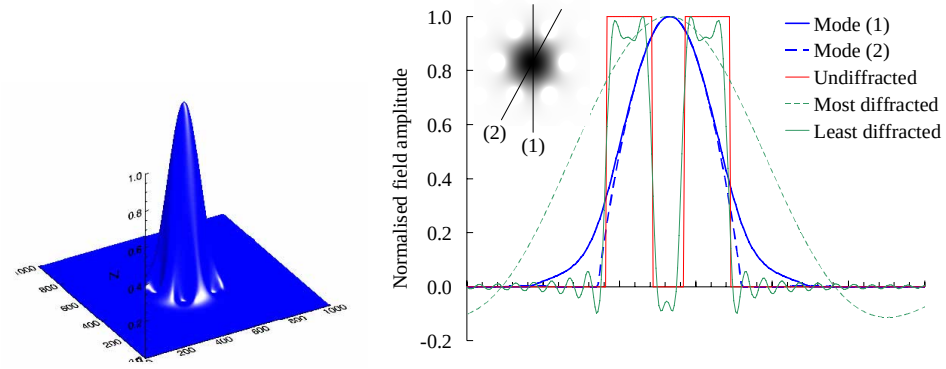

Fig. 4. Cross section through the fiber mode ($|\mathbf{E}_f|$ shown in 3D) and various images of the pupil at the endface of the fiber

Figure 5 shows the maximum coupling efficiency, due to an on axis source, *O* in Fig. 2(b), as a function of telescope exit pupil image size, d_p, telescope obscuration and lateral offset of the pupil image wrt to the mode field of the fiber. These figures represent maximum coupling efficiencies since off axis sources couple less efficiently due to the phase mismatch between $\mathbf{E}_d$ and $\mathbf{E}_f$. (Section 3.2).

In Fig. 5(a), the maximum coupling values change between the least and most diffracted cases due to the affect of $\mathbf{h}(p,q)$ as it scales with respect to $\mathbf{E}_g$. The least diffracted curve peaks at 1.33Λ with the most diffracted image of interest, taken as ρ_{max} >50%, showing a very weak dependence on image diameter, due to the dominance of the lenslet PSF over the image scale in these cases.

#7947 - $15.00 USD Received 27 June 2005; revised 11 August 2005; accepted 11 August 2005

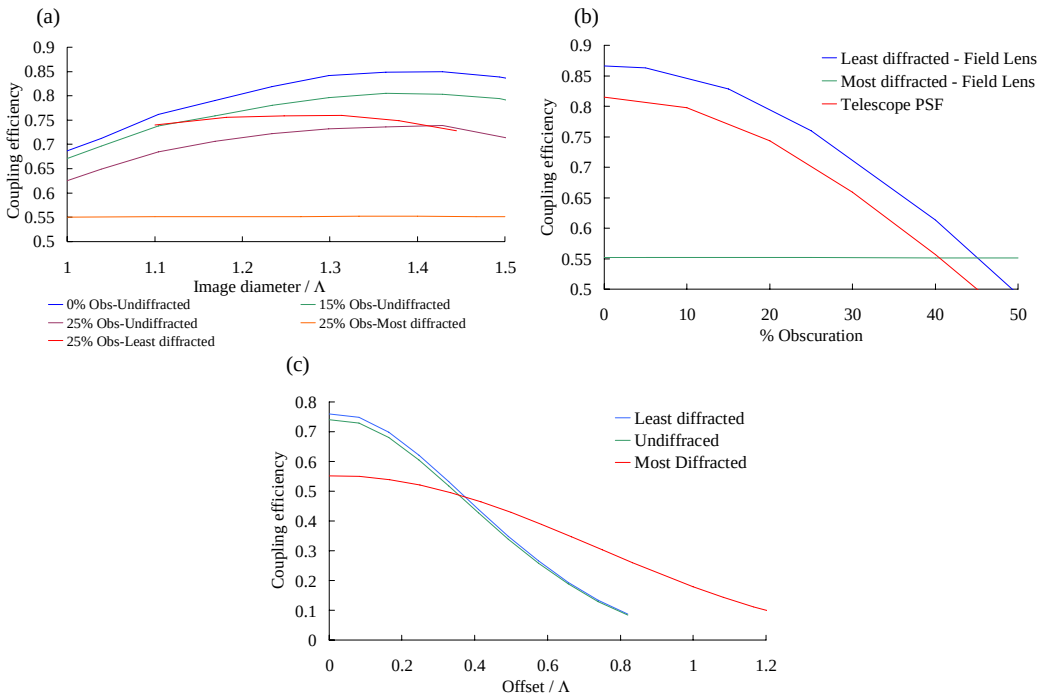

Fig. 5. (a) Maximum coupling, ρ_{max} (i.e.on axis O, in fig 2) characteristics as a function of pupil image scale, (b) $\rho_{max,}$ as a function of telescope obscuration, (c) $\rho_{max,}$ as a function of pupil offset for geometric, diffracted and badly diffracted cases. For a lenslet not in contact with the fiber, these values must be reduced by the Fresnel coefficient at noted in section 2.0.

Increasing obscuration reduces coupling as shown in Fig.5(b), as the mismatch between the missing central portion of the primary image and the centrally located mode becomes more severe. Fig. 5(c) shows that the coupling is highly sensitive to lateral alignment of the pupil image and the fiber mode. A drop in maximum coupling efficiency of approximately 10% occurs for only a 0.25Λ lateral shift and for an LMA-8 fiber this equates to an alignment precision between fiber and lenslet axes of ~1.6μm rising to a few microns for the LMA-20. Alignment tolerances of this order are discussed by Liu *et al* [13] and whilst technologically challenging, are possible.

The values of maximum (on-axis) coupling efficiency with wavelength for various feed focal ratios into the pupil image are investigated with comparison to the direct feed case in section 4.

3.1.1 Gaussian apodisation

Gaussian (amplitude) apodisation of the pupil image was attempted in order to increase the coupling efficiency into the LMA mode which, itself, can be approximated as a Gaussian in the region inside the holey structure [14]. Figure 6 shows the result of increasing the Gaussian half width of the apodising screen with respect to the diameter of the pupil image, d_p (each pair of curves) and of increasing the size of d_p wrt to the static mode field of the LMA fiber (the three sets of curves). Both the transmission and coupling curves are asymptotic to the x-axis and hence Gaussian apodisation works to reduce the overall coupling.

#7947 - $15.00 USD Received 27 June 2005; revised 11 August 2005; accepted 11 August 2005

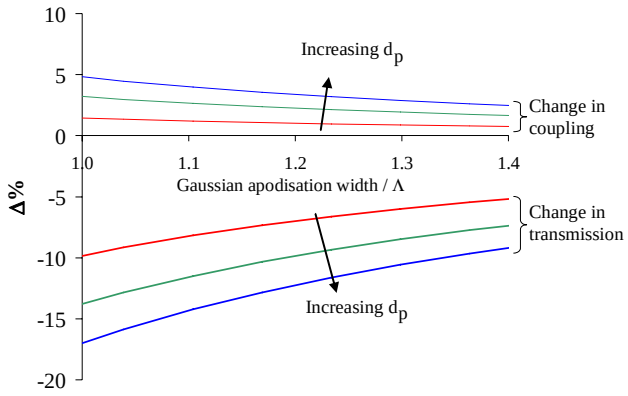

Fig. 6. Effect of Gaussian pupil apodisation on the overall throughput. The three curve sets are for increasing values of d_p, the diameter of the geometric pupil image, $\mathbf{E}_g$ on the endface of the fiber wrt to the static mode field of the LMA fiber.

3.2 - Off axis source.

Referring to Fig. 2(b), the pupil of the telescope illuminated by an off-axis source, *O*, and its *geometrical* image on the fiber endface can be modeled (in one arbitrary polarisation state, along the y-axis, say) as a flat obscured disc, **P**, modulated by a cos term in λ, n ,θ the angle *at the fiber* associated with the off axis source *O* and *y*, the distance from the telescope axis, yielding a term $\mathbf{P}.\exp(ikny\theta)$. Variables, *y* and θ are then linearly related and the much reduced magnitude of y across the extents of the image w.r.t. to the enormous values of *y* in the telescope pupil can be matched by the exact reciprocal scaling in θ for the same value of the exponential term. This is simply an expression of the Smith-Hemholtz invariant[15] for the telescope exit pupil and its (geometrical) image due to the invariance of λ in all space (subject to bulk changes in refractive index, *n*).

As θ increases a phase mismatch between the fiber and incident fields occurs which causes the coupling efficiency to fall off in the manner shown in Fig. 7. The fiber coupling field of view is then defined as the angle at which the coupling efficiency, $\rho_f(\theta)$ falls below some absolute value.

As noted in the previous section, the PSF of the telescope will vignetted, even at θ = 0, by the lenslet aperture and indeed one can view this process as giving rise to the diffraction in the pupil image on the fiber endface [8]. Further, the amount of energy lost to this process will, of course, increase as the telescope PSF is displaced in i' wrt to the lenslet, for off axis sources and so the total field of view can be expressed as

$$\rho(\theta) = \rho_f(\theta).\rho_s(\theta) \tag{7}$$

where the subscripts f and s refer to the fiber coupling efficiency and the loss due to the lenslet aperture stop.

Any constant amplitude terms in $\mathbf{E}_i$, for instance the amplitude of **h** or $\mathbf{E}_g$, cancel top and bottom in Eq. (1) and the power relationship between $\mathbf{E}_d$ and $\mathbf{E}_f$ is lost leaving only ρ_f, the *ratio* of the powers in $\mathbf{E}_i$ and $\mathbf{E}_f$. For instance if $\rho_f = 0.5$ then 50% of the energy incident at the endface of the fiber is coupled into the fiber. The power ratio between $\mathbf{E}_d$ and $\mathbf{E}_i$ is then given by ρ_s and the total throughput from telescope entrance pupil to fiber mode by Eq. (7). The separation of the two terms on the RHS of Eq. (7) is therefore justified and further, whose individual derivations are physically relevant and instructive, see sections 3.2.1/3.2.2. $\rho(\theta)$ itself is investigated in section 4.

#7947 - $15.00 USD Received 27 June 2005; revised 11 August 2005; accepted 11 August 2005

Equation (1) is valid over a restricted range of input angles θ, for which θ^2 is negligible [7,16] at the fiber, however this restriction is not an issue for this application.

3.2.1 – Coupling due to the fiber, $\rho_f(\theta)$

Figures 7(a) and 7(b) show the $\rho_f(\theta)$ characteristics for coupling into an LMA-8 and LMA-15 fiber.

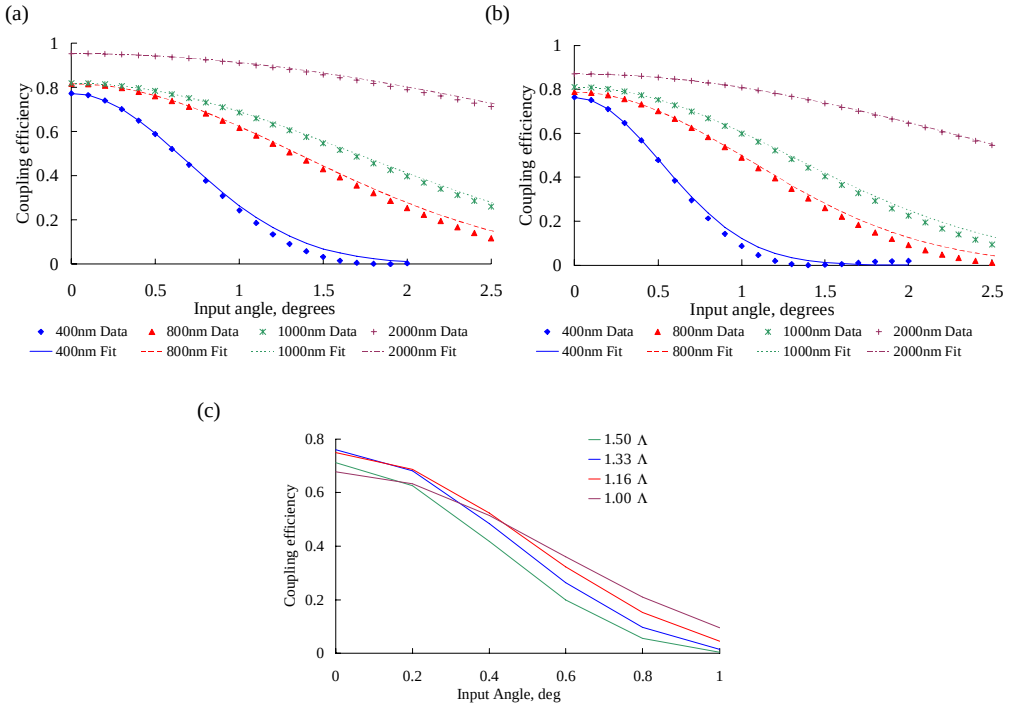

Fig. 7. Coupling efficiencies as a function of input angle for (a) LMA-8, (b) LMA-15 for d_p = 1.33Λ and (c) as a function of d_p. All angles are given in degrees at the fiber endface.

A fit to the curves, accurate to a few percent for $\rho > 0.3$, and lenslet $F_L < 4$ [17] is overplotted in Fig. 7, given by

$$\rho_f(\theta) = \rho_{\max} \cdot \exp\left[-\frac{\theta\left(n/n_{core}\right)^2}{2\left(\beta\left(\lambda_o/n\Lambda\right)\right)^2} \right] \tag{8}$$

where, $\rho_{\max} = \rho_f(\theta=0)$ is the maximum coupling value, n is the refractive index at the fiber endface, n_{core} is the refractive index of the fiber core, Λ is the characteristic length of the photonic structure in the fiber, λ_o is the free space wavelength and β is a numerical constant of value 13.832 when θ is in degrees. As noted in section 3.1, $\rho_{\max}$ changes due to the wavelength dependent scaling of **h** with respect to $\mathbf{E}_g$ in Eq. (6).

Figure 7(c) is a plot of $\rho(\theta)$ for various pupil image sizes, d_p, on the fiber endface. From the plot, $\rho(\theta)$ can be increased/decreased slightly with a corresponding decrease/increase in image size. However, the FOV on the sky is a function of $\rho(\theta)$ and d_p (See Eq. (12)) and the optimum $\rho_{\max} \times \rho(\theta)$ is found at a d_p of 1.33Λ.

#7947 - $15.00 USD Received 27 June 2005; revised 11 August 2005; accepted 11 August 2005

In terms of the fractional loss of efficiency, where $\{\gamma \in [0.0,1.0]: \gamma < \rho_{\max}\}$, (8) can be rearranged to yield,

$$\theta = \frac{n_{core}}{n^2}\beta\left(\frac{\lambda_o}{\Lambda}\right)\sqrt{-2\ln\left(1-\gamma/\rho_{\max}\right)} \tag{9}$$

and since $F = 1/2\theta$ and converting from radians to degrees the associated focal ratio at the fiber,

$$F_{fibre} = \frac{90n^2\Lambda}{\beta\pi n_{core}\lambda_o\sqrt{-2\ln\left(1-\gamma/\rho_{max}\right)}} \tag{10}$$

Now that we have typical values for the required geometric pupil image size and feed focal ratio to the fiber we can calculate the fiber field of view *on the sky* for the given telescope configuration. In Fig. 2(a), the Smith-Hemholtz invariant can be used to derive the angular scale between the telescope exit pupil and its geometrical image such that

$$\frac{nd_p}{n_T d_T} = \chi F_{fibre} \Rightarrow \chi = \left(\frac{n}{n_T}\right)\frac{d_p}{F_{fibre}d_T} \tag{11}$$

(11) is the angular relationship between fiber and sky and holds regardless of the fact the image on the endface of the fiber is diffracted.

Substituting in F_{fiber}, the critical focal ratio associated with a maximum coupling loss of ρ_{max}-γ yields and $d_p = 1.33\Lambda$,

$$\chi = \left(\frac{n_{core}}{n.n_T}\right)\frac{1.33\beta\pi\lambda_o\sqrt{-2\ln\left(1-\gamma/\rho_{max}\right)}}{90d_T} \tag{12}$$

and in units of the angular un-obscured Rayleigh length, $i_R' = 1.22\lambda_o/nd_T$

$$\chi/i_R' = \left(\frac{n_{core}}{n_T}\right)0.5263\sqrt{-2\ln\left(1-\gamma/\rho_{max}\right)} \tag{13}$$

Equation (13) is an extremely interesting result since it says that when feeding the single-mode LMA fiber with a field lens, Fig. 2(a), the *sample size on the sky is independent of the size of the fiber core*, associated with the characteristic size of the fiber, Λ. This result can be understood on the basis that a larger core implies a larger $|y_{\max}|$ in $\exp(ikny\theta)$ and therefore requires a smaller θ for the same value of this term. Therefore as the core grows, the maximum input angle (for the same λ) gets proportionately smaller and hence χ remains constant.

The image plane (i to i') magnification of the foreoptics, M can also be computed using $M = d_i'/d_i = d_i'/\chi f_T$ where f_T is the focal length of the telescope and substituting in (13) yields

$$M \cong \left(\frac{n_T}{n}\right)\frac{d_L'}{1.33\Lambda}\left(\frac{F_L}{F_T}\right) \tag{14}$$

#7947 - $15.00 USD Received 27 June 2005; revised 11 August 2005; accepted 11 August 2005

d'$_L$ is the total aperture size in metres of the lenslet of focal ratio F_L, where the approximation that the minimum focal ratio into the pupil image on the endface of the fiber is that of the lenslet itself, since $Z_v << Z_u$ in Fig. 2.

So to keep M to a reasonable figure, say ≤10 and assuming that $F_L \leq 2$ then for an LMA-8 fiber, $d_L \leq 260\mu m$ for $F_T = 7$ and $d_L \leq 600\mu m$ for $F_T = 16$, assuming that $n = 1.00$ and $d_L \leq 600\mu m$ for $F_T = 7$ and $d_L \leq 1400\mu m$ for $F_T = 16$ for the LMA-20. So significant foreoptics magnifications are required to implement the pupil imaging scheme with a macroscopic field lens with lower M required for smaller lenslets of course.

3.2.2 – Coupling due to the lenslet, $\rho_s(\theta)$

As the telescope PSF moves over the plane of i' it is stopped by the finite aperture of the field lens and this creates an extra term ρ_s in the off axis coupling efficiency. ρ_s can be computed for any aperture using,

$$\rho_s = \frac{\int_{Aperture} |U(\mathbf{r} - \delta\mathbf{r})|^2 d\mathbf{r}}{\int_{Allspace} |U(\mathbf{r})|^2 d\mathbf{r}} \tag{15}$$

which is simply the ratio of energy passed through the lenslet as a fraction of the total field energy, where U is the Airy pattern as specified by (2), and $\delta\mathbf{r}$ is the offset in i' of the centre of U from the telescope axis, dropped from the denominator since integrated over the infinite plane.

4. Comparison of direct and field lens coupling

In this section we bring together effects of ρ_f and ρ_s on the coupling into the fiber using a field lenslet and compare these results with the case where the telescope PSF is fed directly into the fiber.

The sample size of the fiber in i' Rayleigh lengths is given by Eq. (13) and so the sample size of the lenslet in i'can be usefully expressed as

$$S = \chi \Big/ i_R' \frac{F_{fibre}}{F_L} = \frac{1.0902n}{F_L}\left(\frac{\Lambda}{\lambda_o}\right) \tag{16}$$

where S is the number of Rayleigh lengths of the telescope PSF free space wavelength, λ_o, sampled *by the lenslet*. The numerical constant in Eq. (17) subsumes the values of $1.33d_p$, π and the conversion from degrees to radians. Note that since Eq. (16) is the sample size of the lenslet then it natural that it should have no dependence on γor $\rho_{\max}$.

From Eq. (16), the smallest S and hence the largest effect of Eq. (16) occurs for the smallest Λ. Figure 8(a) is an overplot of ρ_s and ρ_f for the LMA-8 fiber with $F_L = 2$, with a telescope obscuration of 25%. Looking first at the on-axis, $\theta = 0$ values, the fiber coupling ρ_F ~96% at 2000nm is due to the excellent match of the *f*/2 PSF at this wavelength and the fiber mode however, the value of ρ_s at this wavelength is 76% yielding the total coupling of ~73%. However, at 400nm ρ_F has a value of ~75% but a ρ_s of 96% and so as the fiber coupling, ρ_F increases with increasing wavelength, the maximum (on-axis) lenslet coupling, ρ_s decreases at approximately the same rate leaving $\rho(0)$ in Fig. 7(b) essentially flat across the whole of the visible–NIR.

Compare this with the coupling characteristics of the direct feed case, computed using Eq. (1) and Eq. (2), overplotted with the field lens curves in Fig. 8(b) where the shape of the coupling curve is due to the wavelength dependent telescope PSF coupling into the wavelength independent mode field of the LMA fiber. From Fig. 5(b), the maximum lenslet

#7947 - $15.00 USD Received 27 June 2005; revised 11 August 2005; accepted 11 August 2005

and direct feed coupling efficiencies are approximately the same for different values of the telescope obscuration.

The fiber mode of a step index fiber is also wavelength dependent and it is possible to arrange a relatively flat response with a direct feed however, the attenuation spectrum of a typical step index fiber that is single-moded at 400nm is very limited [5] whereas the LMA fiber has low attenuation over the whole visible & NIR range and so only the LMA fiber, when fed with a lenslet can be used to couple the entire visible-NIR with a single fiber.

Note from Fig. 8(b), that the *f*/3 lenslet causes ρ_s to fall off in the NIR for the LMA-8 but with the slower lenslet having little affect on the LMA-15.

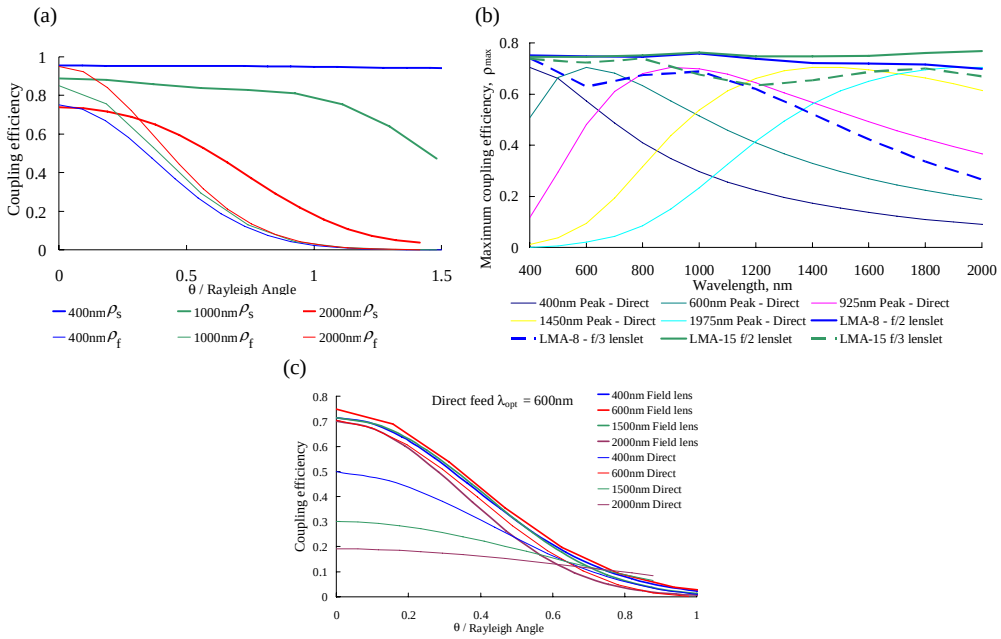

Fig. 8. (a) An overplot of ρ_f and ρ_s for F_L = 2 and an LMA-8 fiber. (b) Overplot of the spectral response of lenslet and direct feed (on-axis) coupling into an LMA fiber for a 25% obscured pupil (c) Comparison of direct and lenslet feed FOV for ρ against θ.

Figure 8(c) is an overplot of the direct feed FOV optimised for maximum coupling at 600nm and of the case of a lenslet feed as given by Eq. (7). The lenslet-fed FOV is constant at the same maximum value of λ/d_T as the direct feed case as shown by the good overplot of the lenslet feed and 600nm direct fed curves. This is also the same FOV as the direct feed into a step index fiber [18].

The reason for the constant FOV of the lenslet feed can be seen in Fig. 8(a) where ρ_s becomes more restrictive in angle at higher λ, whereas ρ_f becomes more restrictive at lower wavelength. These two terms trade off one another in (7) to yield the curves in the Fig. 8(c).

The FOV of the direct feed increases for higher λ when defined on a relative scale of some fraction of ρ_{max} but at the significant cost of nearly ¼ the peak throughput of that associated with the optimum wavelength (600nm in this case) and so the lenslet feed into an LMA fiber makes the entire visible-NIR simultaneously accessible with a both constant FOV and high throughput.

5. Summary

The field lens feeds into an on-axis LMA fiber have been quantified. The LMA fiber is characterised by a large mode field that can be taken as constant in size and distribution with

#7947 - $15.00 USD Received 27 June 2005; revised 11 August 2005; accepted 11 August 2005

wavelength in this application allowing high efficiency coupling of starlight over a much broader wavelength range using a lenslet than the direct feed case.

Step index fibers, with their wavelength dependent mode field, can be used to flatten the direct feed response over an octave or so [12], but generally have severely limited attenuation spectrum by contrast to the LMA case. The maximum field of view of the lenslet fed LMA fiber has been shown to be approximately the same as the direct feed step index and LMA fiber cases.

#7947 - $15.00 USD Received 27 June 2005; revised 11 August 2005; accepted 11 August 2005